Boundary-Layer Meteorol (2013) 147:301–327
DOI 10.1007/s10546-012-9786-6

ARTICLE

Urban Morphology Influence on Urban Albedo: A Revisit with the SOLENE Model

Dominique Groleau · Patrice G. Mestayer

Received: 12 April 2012 / Accepted: 16 November 2012 / Published online: 20 December 2012

Abstract This heuristic study of the urban morphology influence on urban albedo is based on some 3,500 simulations with the SOLENE model. The studied configurations include square blocks in regular and staggered rows, rectangular blocks with different street widths, cross-shaped blocks, infinite street canyons and several actual districts in Marseilles, Toulouse and Nantes, France. The scanned variables are plan density, facade density, building height, layout orientation, latitude, date and time of the day. The sky-view factors of the ground and canopy surfaces are also considered. This study demonstrates the significance of the facade density, in addition to the built plan density, as the explanatory geometrical factor to characterize the urban morphology, rather than building height. On the basis of these albedo calculations the puzzling results of Kondo et al. (Boundary-Layer Meteorol 100:225–242, 2001) for the influence of building height are explained, and the plan density influence is quantitatively assessed. It is shown that the albedo relationship with plan and facade densities obtained with the regular square plot configuration may be considered as a reference for all other configurations, with the exception of the infinite street canyon that shows systematic differences for the lower plan densities. The curves representing this empirical relationship may be used as a sort of abacus for all other geometries while an approximate simple mathematical model is proposed, as well as relationships between the albedo and sky-view factors.

Keywords Albedo · Radiation trapping · Shortwave radiation · Sky-view factor · Urban albedo · Urban climate · Urban form

D. Groleau
École Nationale Supérieure d'Architecture de Nantes, CERMA UMR CNRS 1563, LUNAM Université, 6 quai François Mitterrand, BP 16202, 44262 Nantes Cedex 2, France
e-mail: dominique.groleau@cerma.archi.fr

P. G. Mestayer (✉)
CNRS, Institute for Research on Urban Sciences and Techniques—IRSTV FR CNRS 2488, LUNAM Université, BP 92104, 44321 Nantes Cedex 03, France
e-mail: patrice.mestayer@ec-nantes.fr

1 Introduction

The urban albedo A is the primary characteristic determining the thermodynamics of an urban area since $1 - A$ is the part of the solar energy that is input into this thermodynamic system and partially transformed into sensible heat. It is dependent, on the one hand, on the albedos a_i of the various surface materials, and on the other hand on the three-dimensional (3D) urban form, or morphology, which is responsible for the fractions of sunlit and shadowed surfaces and on the solar radiation trapping. The influence of the urban morphology on the urban climatology and neighbourhood micro-climatology is complex and the urban form may have unexpected and even adverse influences as in, e.g. the urban heat island (UHI), which may not only increase the impact of summer heat waves but also reduce the winter heating load of buildings. This complexity is largely linked to the non-linearity of radiation and heat transfer processes that intervene in the urban energy balance. Most of these processes depend on the component surface temperatures with different and somewhat opposed dependencies: infrared emission and reflection; heat transfer by convection in the air, by conduction in the solid materials and by evapotranspiration; and with the addition of anthropogenic heat releases (Oke 1987, 1988; Masson 2006). It is, therefore, very difficult to take into account all these microclimatic influences when designing the morphology of an urban project respecting the various facets of sustainable development. This usually requires the operation of a rather complete and complex thermo-radiative model adapted to the designed geometry and taking into account the building structure and environment, the energy consumption practices and a large panel of climatic conditions. It is, therefore, appealing to compute separately the influence of the morphology on the absorption of solar energy because (1) it is the primary input of the urban thermodynamic system and (2) it is not dependent on the other energy transfer processes and can, therefore, be studied in isolation.

The urban fabrics reflect less solar radiation than horizontal surfaces with the same reflectivities because of the solar radiation trapping that is generated by the multiple reflections of the radiation within the 3D geometry, generating in turn an increased energy absorption. Hereunder, to avoid confusion, we use the word albedo for the effective reflection coefficient of the whole urban fabric, A, and reflectivity for the individual facet surfaces, a_i. The first heuristic study of multiple reflections within urban-like geometries included both model measurements (Aida 1982) and numerical simulation using a two-dimensional (2D) Monte-Carlo method applied to a 2D urban block-canyon geometry (Aida and Gotoh 1982). Arnfield simulated the Aida (1982) experiment with a canyon radiation model based on the radiosity method with respective view factors of street facets (see Arnfield 1988). Kondo et al. (2001) used a photon tracking method based on Monte Carlo calculations applied to a regular lattice of cubic buildings of equal sizes. Sievers and Zdunkowski (1985) developed an analytical algorithm for an infinite number of reflections within one infinite street canyon. Masson (2000) used a similar approach for his surface energy budget (SEB) model, with the assumption of a street direction isotropic distribution. Groleau et al. (2003) presented the first effective albedo calculations for a real district, with the model SOLENE based on the radiosity approach with an unstructured computational grid. Kanda et al. (2005) developed an approach, based on building-face view factors and sunlit-shadow distributions, which is 'simple' but restricted to an infinitely extended regular array of uniform cubic buildings. They also extended the Aida (1982) experiment over large arrays of 0.15-m cubic concrete blocks. Finally, Krayenhoff and Voogt (2007) introduced also in their SEB model TUF-3D a radiosity calculation based on a regular grid of square patches. Note that these models differ not only by the calculation methods but also by the surface reflection assumptions (including diffuse reflections of Lambertian surfaces and including or excluding specular reflections)

and by the solar radiation inputs. We refer to Krayenhoff and Voogt (2007) for an analysis of the sources of errors in the measurements and in the different simulation methods.

However interesting these novel model presentations may be, unfortunately most of the above works did not much improve our knowledge of morphology influence on the albedo, either because their results are restricted to comparisons with earlier works, or because they concern cases with different reflectivities for roofs, walls and grounds that mingle influences. For instance, Pawlak and Fortuniak (2002) compared an analytical solution of multiple reflections to 2D Monte Carlo simulations for a large series of street-canyon cases (parallel or perpendicular to the sun's direction) as a function of canyon aspect ratio with identical road and wall reflectivities ($a = 0.40$) but another series is based on different reflectivities and, like the previous similar calculations of Masson (2000), their calculations do not include roofs. Therefore, most of our knowledge on the influence of morphology was provided by the measurements of Aida (1982) and the heuristic simulations of Kondo et al. (2001), although additions and analyses of other authors are not negligible. For instance, Oke (1988) popularized the results of the earlier studies, especially those of Aida and Gotoh (1982), and gave to many readers the impression that the urban albedo varies not only as a function of geometrical factors but also largely with solar elevation angle, hence with the diurnal and seasonal cycles. Yet, more recent on-site measurements and simulations at the neighbourhood scale reported by Christen (2005), Idczak et al. (2010), Hénon et al. (2011, 2012) yield weak variations of the albedo with the diurnal cycle as well as with the annual cycle.

In conclusion, what do we know about purely geometrical influences? Let us first consider the configuration of block arrays:

- the albedo decreases monotonically with the increasing building height, at least for a building plan density of 0.25 (Aida 1982; Kondo et al. 2001);
- the albedo decreases slightly when the building height is not uniform (Kondo et al. 2001);
- the albedo diurnal cycle depends on the array orientation in a complex manner, with no clear trend for its average value (Aida 1982; Kondo et al. 2001; Kanda et al. 2005);
- the albedo depends on the building plan density, but not monotonously (at least for the building height of 25 m) and the relationship is still unknown (Kondo et al. 2001; Kanda et al. 2005; Krayenhoff and Voogt 2007);
- the diurnal and seasonal variations are uncertain since the observed variations with sun elevation show important differences, in shape and amplitude, according to the authors and models, some of which are unrealistic (Kondo et al. 2001; Kanda et al. 2005; Krayenhoff and Voogt 2007);
- the albedo and sky-view factors are certainly related (Kondo et al. 2001) but the relationship is still unknown.

As concerns the street canyon geometry (with no roof):

- the albedo decreases with increasing height-to-width aspect ratio (Aida and Gotoh 1982; Sievers and Zdunkowski 1985);
- the albedo diurnal variation depends on street orientation (Aida 1982; Aida and Gotoh 1982; Sievers and Zdunkowski 1985);
- with increasing solar elevation the albedo increases when the aspect ratio is low and decreases when it is high, the crossing point depending on the diffuse-to-direct radiation ratio (Masson 2000; Pawlak and Fortuniak 2002);
- the absence of roofs and crossroads certainly induces a systematic bias with respect to real urban fabrics (Krayenhoff and Voogt 2007).

In view of these conclusions it is clear that the morphology does influence the urban albedo but the relationships between albedo and geometrical factors are still very unclear,

generally limited to trends and with no algebraic representation. The problem deserves the present reconsideration, using the powerful SOLENE model that allows simulation of the thermo-radiative behaviour of an urban neighbourhood of any regular or irregular shape, hence schematic or realistic geometries. SOLENE has been largely used during 10 years of architectural, environmental and climatologic studies and it has recently been validated against measurements of several on-site experiments (see references in Hénon et al. 2012).

One of the most remarkable, and desirable, characteristics of urban morphology is the large diversity and heterogeneity, from one city to another as well as within one urban area. To produce heuristic relationships between urban albedo and form it is, therefore, necessary to reduce the morphology to a small number of pertinent geometrical factors. The most often used geometrical factors are plan area density, frontal area index, street aspect ratio, building form factor(s) and sky-view factor(s), some of them with different definitions according to author. The choice of these factors is strongly related to the generic scheme used to represent the canopy geometry. The most commonly used urban schemes are: (1) the infinite array of identical parallelepiped building blocks, hereunder the 'Plot' geometry and (2) the array of parallel homogeneous street canyons composed of infinitely long bars of buildings, hereunder the 'Canyon' geometry. Unfortunately, the characteristic factors of these schemes are usually: (i) not compatible with another geometry; (ii) not representative of real geometries as, e.g. non-orthogonal layouts, backyards, alleys and open squares; and (iii) often not pertinent or difficult to obtain in the architectural/urbanistic design process. Two geometrical factors intervene evidently in the radiation trapping process: the built density or conversely the un-built density; canopy fraction allowing solar radiation to penetrate; and the building heights that determine the fraction of surfaces in shade, the number of radiation reflections and the sky-view factors from the ground and facades. On the one hand, the usual plan density has values clearly limited between 0 and 1, but on the other hand the limit to the building height is unknown (as seen with the recent prestigious towers reaching several hundred metres) that is a default for a complete heuristic study. The aspect ratios based on building heights have evidently the same default.

After preliminary parametrical studies we propose to introduce a more pertinent geometrical factor: the facade density. It reconciles the previous factors, keeps the same significance for all geometries, either idealised or realistic, and is easy to compute. Therefore, the present analysis is based on the two main geometrical non-dimensional factors, plan density d_p and facade density d_f, here defined as :

$$d_\mathrm{p} = A_\mathrm{B}/A_\mathrm{T}, \tag{1}$$

$$d_\mathrm{f} = A_\mathrm{F}/(A_\mathrm{F} + A_\mathrm{R} + A_\mathrm{G}), \tag{2}$$

$$A_\mathrm{B} = \sum_{i=1}^{N} A_{\mathrm{b}i}, \tag{3a}$$

$$A_\mathrm{R} = \sum_{i=1}^{N} A_{\mathrm{r}i}, \tag{3b}$$

$$A_\mathrm{F} = \sum_{j=1}^{M} A_{\mathrm{f}j}, \tag{3c}$$

$$A_\mathrm{G} = \sum_{k=1}^{P} A_{\mathrm{g}k}, \tag{3d}$$

$$A_\mathrm{T} = A_\mathrm{B} + A_\mathrm{G}, \tag{3e}$$

where A_B, A_G and A_T are the built, un-built (ground) and total plan areas of the scene or territory, respectively, A_R and A_F are the total surfaces of roofs and facades, A_{bi} and A_{ri} are the plan area and roof area of building i, A_{fj} is the area of building facade j, A_{gk} is the plan area of ground lot k, N, M and P are the numbers of buildings, building facades and un-built lots in the scene, respectively. Thus d_f is the ratio of the area of facades to the area of the total urban envelope (or folded surface). Both d_p and d_f vary between 0 and 1 and the facade density increases with the building height. The building compactness, i.e. the ratio of the perimeter to the surface, may also participate in the variation of d_f, but it may be a secondary parameter.

With the assumption of flat roofs ($A_{bi} = A_{ri}$) the facade density becomes

$$d_{\text{f-flat roof}} = A_F/(A_F + A_T). \tag{4}$$

In this case, these two densities may be related to the usual geometrical factors for the Plot geometry

$$d_{\text{p-Plot}} = L_x L_y/A_T, \tag{5a}$$

$$d_{\text{f-Plot}} = 2\left(L_x + L_y\right) H/\left[A_T + 2\left(L_x + L_y\right) H\right], \tag{5b}$$

as well as for the Canyon geometry

$$d_{\text{p-Canyon}} = W/(W + W_b), \tag{6a}$$

$$d_{\text{f-Canyon}} = 2H/(2H + W + W_b), \tag{6b}$$

where L_x and L_y are the block length and width, W and W_b are the street and building bar widths, H is the building height. Note that $d_{\text{f-flat roof}}$ differs from the facade or frontal area index, often defined as A_F/A_T, which has the shortcoming of having no upper limit.

To normalize the influence of the morphology independently of the individual surface reflectivities Aida (1982) introduced the 'absorption increment' defined as 'the rate of anomalous absorption by the surface irregularity to the flat surface of the same quality' $(B_i - B_0)/B_0$, where B_i is the absorptivity of model i and B_0 is the absorptivity of the flat model. We also use the urban absorptivity $(1 - A)$, the mean surface absorptivity $(1 - \tilde{a})$ and their difference

$$(1 - A) - (1 - \tilde{a}) = \tilde{a} - A, \tag{7}$$

which indicates the increase of solar radiation absorption due to the urban morphology, compared to what it would be if the city was flat. The mean albedo of the individual surfaces $\tilde{a}$ may take several definitions as, e.g. the average of the albedos of all the surfaces of the urban envelope (roofs, facades and ground surfaces) weighted by their areas (A_{ri}, A_{fj}, A_{gk}) or the average of the albedos of the only roofs and ground surfaces weighted by their plan areas (i.e. the apparent average albedo of the patchwork seen from the sky). Here, to concentrate our study on the only influence of geometry, we use the same reflectivity for all surfaces, which allows us to normalize the albedo results by $\tilde{a}$ without ambiguity.

In the present article we report the main results of our heuristic study of the urban albedo and sky-view factor variations as a function of several morphological variables, obtained from numerical simulations with the SOLENE model. The scanned variables are plan density, facade density, layout type and orientation; and the date and time influences are also considered. In the next Section we briefly present the features of SOLENE that are used in the present study. In Sect. 3 we analyse in detail the results obtained with the generic Plot geometry and propose an approximate, simple model of the relationships between the albedo and the densities. We compare these first results with those obtained with the Canyon geometry in

Sect. 4, and with other geometries in Sect. 5, including actual districts of the city of Nantes. Finally, Sect. 6 gathers our conclusions.

2 Computational Set-up

The albedo computations are performed with the SOLENE model (Miguet and Groleau 2002). The 3D geometry of the folded urban surface is composed of a set of polygonal plane faces on which we apply a grid of triangular meshes (facets), between 1 and 20 m^2 in area for urban canopy simulations. The sky vault is modelled by an additional geodesic hemisphere, composed of 1,024 facets, to take into account the anisotropy of the diffuse solar radiation. The radiation spectrum is divided into solar radiation (0.3–2.5 μm) and infrared thermal radiation (2.5–18 μm); infrared radiation is not considered in this study because its behaviour is coupled with radiation-heat conversions and heat transfers while solar radiation can be simulated in isolation. Note also that these conversion processes require a considerable amount of additional computational load incompatible with a large heuristic study (see, e.g. Vinet 2000 or Hénon et al. 2011). The solar radiation from the sky includes two components, direct and diffuse, where direct radiation is emitted by the sun in the direction of the canopy, according to its azimuth and elevation angles. The diffuse radiation emission is distributed over all sky meshes according to the sky radiance model of Perez et al. (1993); illustrations may be found in Miguet and Groleau (2002) and Idczak et al. (2010). The multiple reflections are computed according to the reflection and transmission properties of the surfaces; in this study the surfaces are opaque and Lambertian, and only their solar reflectivity is considered. This computation uses the radiosity method that first requires the computation of the form factors (solid angles) or view factors between all facets of the surfaces and of the sky vault, taking into account the masking effect of the 3D geometry by a projection method (Vinet 2000; Miguet and Groleau 2002). The form factors of all the facets that are visible from the barycentre of a facet are recorded in the facet information dataset. The information data include also the facet area, the surface reflectivity and also its class (ground, facade, roof), which allows us to compute separately some class area-weighted averages of any property or variable.

The sky-view factor indicates the quantity of sky visible from an observation point. It is computed as the sum of the view factors of the sky-vault facets seen from this mesh, normalized by the solid angle of the hemisphere (2π). The urban albedo is the ratio of the total solar energy reflected towards the sky to the total solar energy emitted by the sky vault. The reflected solar energy is the sum of the solar energy reflected towards the sky by the mesh elements of the urban geometry weighted by their sky-view factor, after computation of the multiple reflections within the urban geometry. If F_i is the value of a variable F associated with the mesh i (e.g. its sky-view factor, solar flux or reflectivity) here the mean value of F is defined as

$$\bar{F}_D = \sum_{i \in D} A_i F_i \Big/ \sum_{i \in D} A_i , \tag{8}$$

where A_i is the area of mesh i and D is the averaging domain of meshes, for instance the ground surfaces. Normally the averaging domain is the analysis domain defined below.

Here the computational conditions are fixed by the following parameters. The incoming solar radiation is computed with the model of Perez et al. (1993) for clearsky conditions with predominant direct solar radiation and diffuse solar radiation concentrated on the sky vault

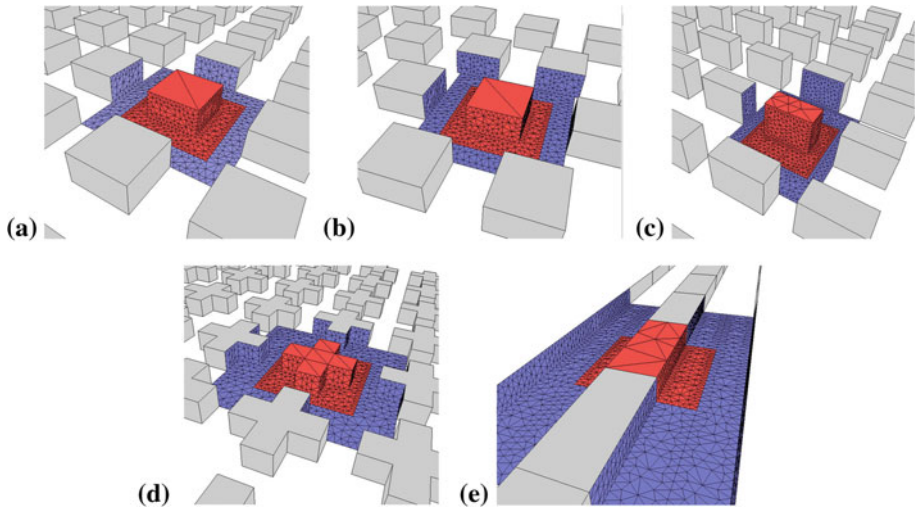

Fig. 1 Sketches of the computational domains of the idealized configurations, with the analysis domain in *red*, the radiosity domain in *blue*, the mask domain in *grey*: **a** regular plot configuration, **b** square plots in staggered rows, **c** rectangular plots, **d** cross plots, **e** street Canyon configuration

in the direction of the sun. The chosen latitude is 45° N, with additional simulations for 35° N. The seasonal and diurnal parameters are selected to demonstrate the solar angle influence: three days representing the seasonal extremes, the winter solstice (December 21), the spring equinox (March 21) and the summer solstice (June 22); for each date, all daytime hours, from 0800–1600, 0700–1700, 0500–1900, respectively (in this study time is local solar time). The plan density d_p and the facade density d_f vary from 0.10 to 0.90 in steps of 0.10, however limited to a maximum building height of about 100 m, while several grid/street orientations are surveyed, aligned with the cardinal points and slanted by 45°, i.e. at 0° and 45° from the north for the symmetrical cases, or at 0°, 45°, 90° and 135° for the unsymmetrical ones. About 270 different geometrical cases are analysed, corresponding to some 3,500 simulations of all daytime hours. To concentrate on geometry influence the surface reflectivity is the same for all surface types such that, except where explicitly indicated, $a_i = \tilde{a} = 0.45$. Although this is a rather high average albedo for actual cities, due notably to the usually low albedo of pavement, this value is chosen with reference to the work of Kondo et al. (2001).

The definition of the computational domain requires attention. Actually for each configuration under study three different domains are defined (Fig. 1). The computation of the results (albedos, sky-view factors) are performed on an analysis domain (red in Fig. 1) that is one element of the periodic geometric grid (one hectare in area for one building), but the intermediate computations require us to enlarge the computational domain to take into account the influence of the neighbouring buildings and ground. For the computation of the multiple reflections the radiosity domain (blue in Fig. 1) includes the closest facades of the four neighbouring buildings and all the ground surface between them. For the computation of the form factors and solar fluxes from/to the sky the mask domain (grey in Fig. 1) is extended further to a number of building rows that depends, in principle, on the built density, to take into account all the intercepting surfaces between the sky and the radiosity domain.

The choice of the mask domain extension is delicate: when too wide it unreasonably increases the computations, but when too short it yields erroneous sky-view factors and

incident solar radiation on the facets of the computation domain. This 'edge effect' is a possible source of error in urban radiation simulations, especially when the albedo is computed as $1 - E_a/E_i$ where E_a is the total energy absorbed by the facets of the analysis domain and E_i is the total incident energy from the sky. Attention is especially required when the building density is low, when the building height is low and when the sun elevation is low. Krayenhoff and Voogt (2007) note also that the error magnitude increases when the calculation resolution is decreased, i.e. when the number of facets is low.

3 Albedo and Sky-View Factors of the Plot Geometry

3.1 The Plot Configuration

The most common generic urban morphology is based on the Plot geometry. Hereunder 'configuration' is used to indicate the plan arrangement of the plots and/or streets and the computational domain and grid, while 'geometry' refers to the real 3D geometrical shape. The structure is built on a regular square grid whose basic element is a 1-ha square, 100 m in length, with a square building in its centre (Fig. 1a). The building lengths and heights are computed with Eqs. 4, 5 to provide the built densities in steps of 0.1. Although this set-up is dimensional it is evident that the computation results are independent of the basic size and would be identical with an homothetic geometry. As urban density increases, the Plot geometry progressively transforms from a set of isolated buildings to a regular array of blocks and street canyons (hereunder 'Plot' is the generic for Plot geometry as defined in the Introduction, and which includes several variants defined in Fig. 1: regular (aligned squares, staggered, rectangular, cross). The variation of the two densities within the above-mentioned limits required 78 Plot simulation cases, and 84 additional ones were needed to document the influences of the other parameters (orientation, staggered rows, reflectivity), simulated for all daytime hours.

The mask domain is set to nine rows in both directions (Fig. 1a). The computational grid is composed of triangular meshes about 5–10 m^2 in area for the grounds and facades, with a higher density of meshes in the analysis domain, while the roofs are composed of only two triangular meshes since they do not give rise to multiple reflections.

As indicated above, some simulations have been repeated with square buildings in staggered rows in place of the regular layout (Fig. 1b). The computational domains are rather similar to those of the regular Plots with the mask domain extending over nine rows and the analysis domain extending over a unit of 1 ha with one building. However, this configuration requires an extended radiosity domain (in blue) since the facades of six neighbouring buildings are implied in the reflection calculations instead of four.

3.2 The Influences of Time, Date and Orientation

The results obtained over the daytime part of the diurnal cycles show very low amplitudes of the diurnal variation. Figure 2 displays results for a series of typical cases with the largest amplitudes over the 78 Plot simulations. The variations of the albedo as a function of d_f are discussed further below and here we concentrate on the variations with time and date. The curves present a maximum at noon for low d_f values and a minimum at noon for higher d_f, with a transition between $d_f = 0.3$ and 0.5. This is well illustrated by the comparison between the four curves for the March simulations with $d_p = 0.5$ and d_f increasing from 0.1 to 0.8, showing a deepening of the midday trough when the building height (and d_f) increases,

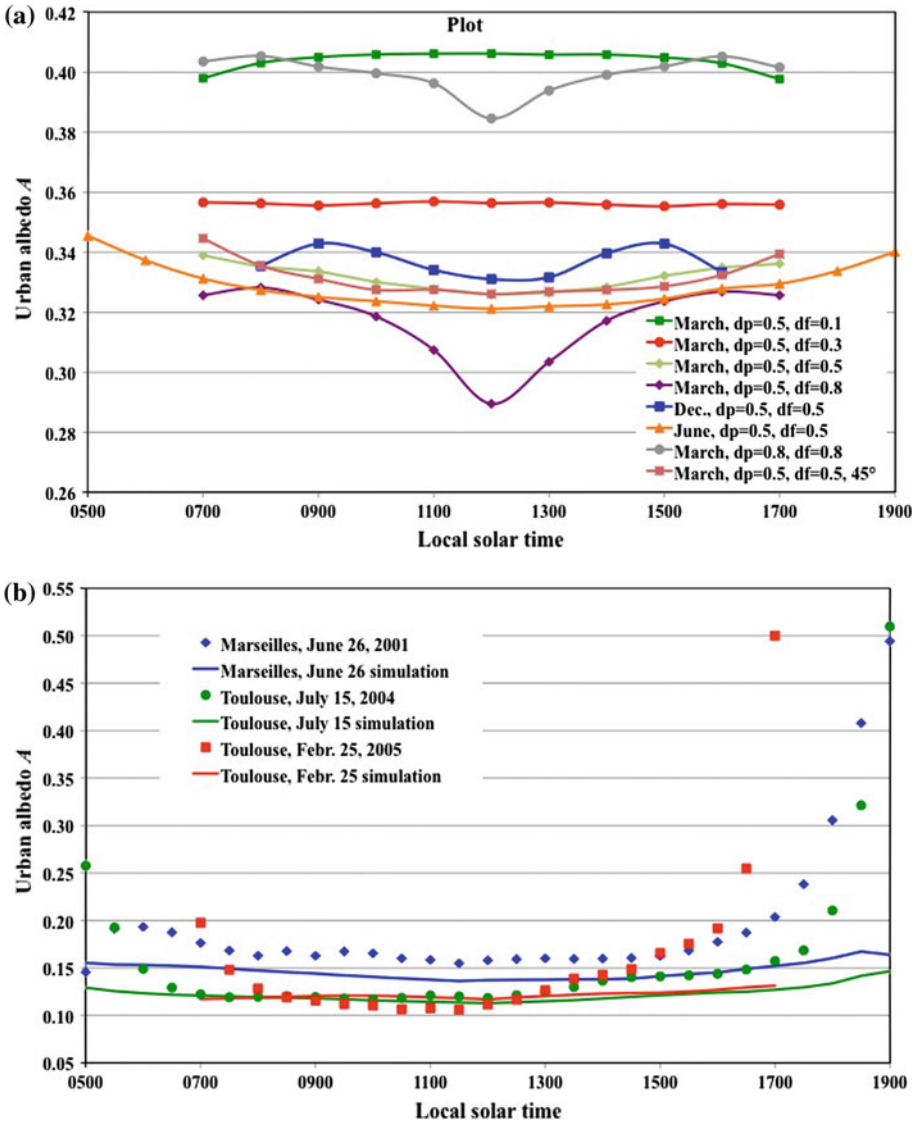

Fig. 2 Urban albedo daytime variations for a selection of Plot simulations (**a**) and for the measurements (*symbols*) and simulations (*lines*) of the Marseilles and Toulouse city centres (**b**); note the difference of scales

because the higher buildings increase the radiation trapping at the times when solar radiation penetrates deeper within the canopy.

Secondly, the comparison of the results of the simulations in December, March and June for the same geometry ($d_p = 0.5$, $d_f = 0.5$) shows that the shape of the curves do change while their mean level is nearly independent of the season: 0.337, 0.332 and 0.329, respectively, i.e. an annual variation of $\pm 1\,\%$. Thirdly, the comparison between the two curves for March and $d_f = 0.8$, with $d_p = 0.5$ and 0.8, does not show a diurnal amplitude increase with the increasing density as in Kanda et al.'s (2005) results. Finally, the comparison between the

two curves for March with $d_p = 0.5$ and $d_f = 0.8$, the first one for the normal orientation and the second for the 45° slanted orientation, shows that the orientation influence is negligible. These conclusions may be repeated for all the simulations that are not shown here for lack of space. For instance, a series of simulations was carried out for the Plot configuration in staggered rows (Fig. 1b) with $d_p = 0.3$ and all d_f values from 0.1 to 0.9: the results yield strictly identical albedo values to those obtained with the regular grid, showing no influence of this set-up. We will discuss this issue further in Sect. 5.

Among all Plot simulation runs the root-mean-square of the albedo diurnal variations is always $<1.5\,\%$ of its daytime average. Although it may seem counter-intuitive and inconsistent with data reported by Kanda et al. (2005), this result is quite consistent with the simulations of Kondo et al. (2001). In Fig. 2b we report the measurements of Grimmond et al. (2004) in the Marseilles city centre and the recent simulations of Hénon et al. (2011) and the measurements of Masson et al. (2008) and Pigeon et al. (2008) in Toulouse, simulated by Hénon et al. (2012). In Marseilles, the levels of measurements and simulations do not match perfectly because they concern neighbouring urban scenes but not exactly the same one: the field of view of Grimmond et al.'s downwards-looking pyranometer includes a noticeable amount of tree crowns, while the simulations consider a four-street block with no vegetation. For the Toulouse city centre, Hénon et al.'s simulations coincide exactly with the actual sensor field of view (location, height and opening angle) and the results agree quite well during the central daytime hours. In all three cases and also in other measurements such as those of Aida (1982) or Christen (2005), a rapid rise in the albedo is observed just before sunset, which is not reproduced in the SOLENE simulations. We believe this is a measurement artefact at a time when both incident and reflected fluxes are very weak. It may be due to any of five causes: (i) additional specular reflections, (ii) artificial city lights, (iii) a slight tilt of a pyranometer, (iv) a different masking influence of the neighbouring buildings on the two radiometers located at the bottom and top of the mast and (v) mainly the difference of horizon at roof and sensor levels since the down-looking pyranometer receives a small but increasing amount of direct solar light during the duration of sunset at roof level (which lasts about 30 min at the equinox and 45 min at the summer solstice, at 45°N). We believe that measurements at sunrise and sunset with two separate radiometers should not be used to infer urban albedos. The results for Marseilles are representative of a pure geometrical influence since roofs and facades have close reflectivities in this scene, 0.23 and 0.25, respectively, and they show a low influence of solar elevation through the diurnal cycle. In contrast, the results for Toulouse illustrate the larger influence of solar elevation when the reflectivities of facades and roofs differ significantly (0.17 and 0.25, respectively), confirming the previous studies referred in Sect. 1, and demonstrating that the influence of albedo differences easily masks that of the geometry.

Although the albedo diurnal variation remains small we observe in Fig. 2 that the shape of the variation curve changes with density and we recognize U-, M- and $\bigcap$-shape curves (i.e. with either a minimum or a maximum at noon) that were also observed in previous studies. To further explore their dependence we have considered the amplitude of the diurnal variation, i.e. the difference between the albedo at noon and the most different albedo in the day such that a positive amplitude indicates a maximum at noon ($\bigcap$-shape) and a negative amplitude indicates a minimum (U- or M-shape). The curves (not shown for lack of space but available on request) are slightly chaotic but they show several clear trends:

- the absolute value of the amplitude exceeds 0.15 only for the highest densities;
- the albedo curves present a maximum at noon for the lower facade densities d_f, only when the plan density d_p is <0.8;

- the noon trough is more pronounced for the highest facade densities;
- the shape of the albedo curve is less dependent on d_f for the higher values of d_p.

In view of these results we conclude that, for the Plot configuration, except for very low solar elevations the solar parameters have small influences on the albedo when morphology is considered alone: (i) the albedo diurnal variations are very limited and (ii) the time of year and latitude influences are marginal. Consequently we consider that it is not necessary to detail here all the further analyses for all times and dates. Therefore, in the following sections, except where explicitly indicated, we analyse only mean albedo values; these mean albedos are actually the averages over all daytime hours at the spring equinox (March 21), which appear to be the most representative values.

3.3 The Influence of Plan and Facade Densities

The mean albedos resulting from the 78 simulations for the Plot geometry appear in Fig. 3 as a function of facade density d_f and plan density d_p. In Fig. 3, the black circles correspond to the Kondo et al. (2001) cases that are discussed in Sect. 3.5. Three observations may be provisionally deduced from these figures: first, with the choice of d_f and d_p as explanatory parameters, the albedo variations are monotonous for all values of the parameters. Second, for a given plan density the urban albedo decreases as the facade density increases, all the more so when the plan density is low. In this context 'facade density' can somewhat be replaced by 'building height' since the facade density increases with the building height when the plan density is fixed. This observation underlines the fact that the influence of building facades on solar trapping increases with their height. Third, for a given facade density the urban albedo increases as the plan density increases, all the more so when the facade density is high. This underlines the increasing contribution of roofs, which do not generate radiation trapping, and the decreasing influence of the canopy depth, which is responsible for the increase in absorptivity. The further observation of the curves of Fig. 3 leads to additional comments, especially their behaviour at the extreme limits. At the one end, when $d_f \to 0$, i.e. the flat city limit with no shadows and no solar radiation trapping, all curves converge towards a maximum that is the value of the average reflectivity of roofs and ground, $\tilde{a}$. At the other end, the general shape of the curves suggest that they tend towards an asymptote when d_f increases, all the more rapidly as d_p is high. This tendency can be understood with a 2D view like Fig. 8a of Oke (1988) or Fig. 1 of Aida and Gotoh (1982) with a variable building height and a constant solar angle. When the building height increases the solar radiation no longer reaches the ground; since most of the multi-reflections take place in the sunlit volume that does not change (for a given sun angle), while only marginal and decreasing reflections take place in the lower parts of the canyons that have very low and decreasing sky visibilities, then the albedo decreases less and less. This evolution is accelerated when the space between the buildings narrows, i.e. when the plan density increases. In contrast, for the lowest building heights the evolution is inversed by the increasing sunlit part of the ground.

This explanation calls for a study of the relationships between albedo and sky-view factors (and geometrical factors). The mean sky-view factors from the ground surfaces F_g and from all the canopy surfaces F_c are presented in Fig. 4a as a function of d_f. These mean factors are the averages computed using Eq. 8. For clarity only the canopy factor curves for $d_p = 0.1$ and 0.9 are presented since they delineate the narrow envelope of the F_c curves obtained for the other values of d_p (grey area). This part of the figure shows that the canopy sky-view factor is strongly dependent on the facade density but only weakly dependent on the built plan density. F_c varies nearly linearly with d_f for the higher plan densities and with an increasing but weak non-linearity with the decreasing d_p. Actually it appears to be surprisingly close to

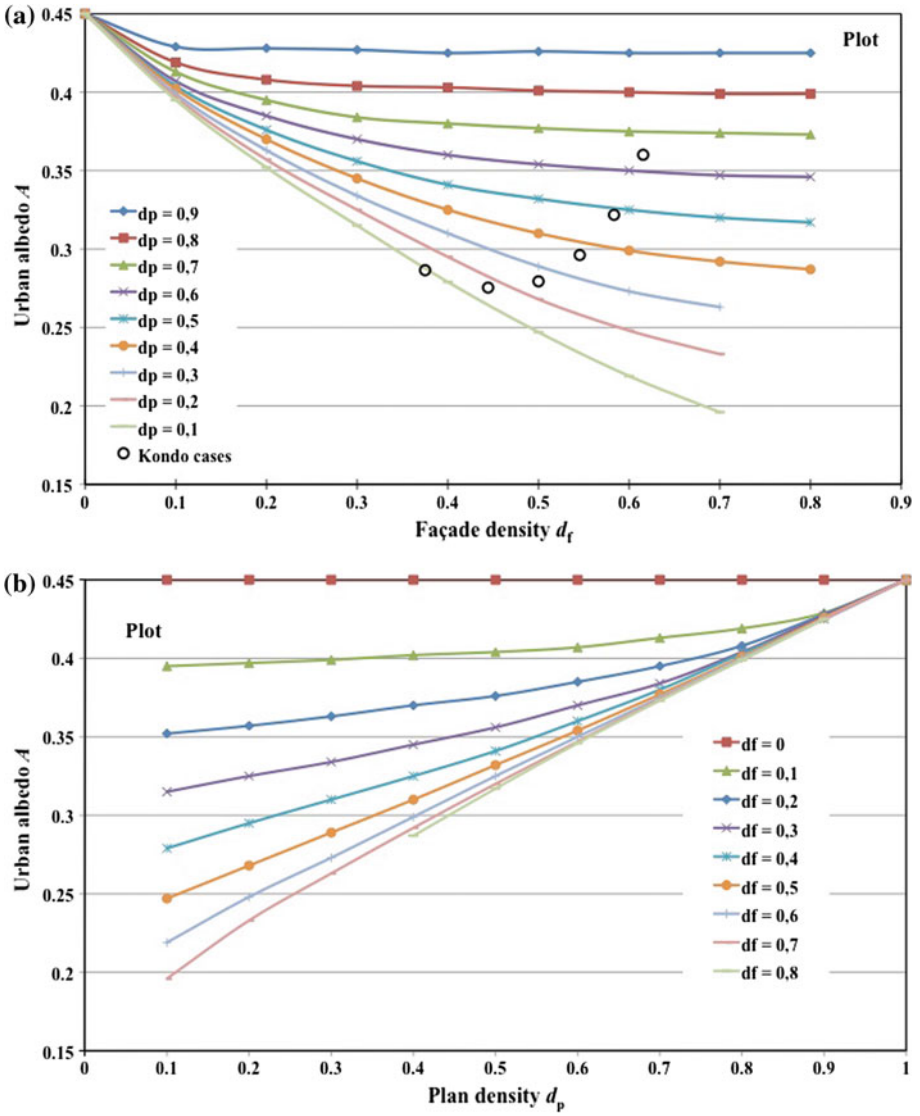

Fig. 3 Variation of the albedo as a function of facade density (**a**) and plan densities (**b**), for the Plot configuration. The data labelled 'Kondo cases' are discussed in Sect. 3.5

the simple linear relationship $F_c = 1 - d_f$ (dash-dot line). As for the ground sky-view factor, F_g, it is seen to decrease with d_f, about linearly for the lowest plan densities and increasingly non-linearly with increasing d_p, reducing more and more rapidly towards zero.

The relationship between the albedo and the ground sky-view factor is illustrated in Fig. 4b; it is seen to be monotonous and depending on the built plan density. The albedo dependency on F_g is moderately non-linear, tending towards a linear relationship for high F_g values (low-to-moderate facade densities) with a slope proportional to $1 - d_p$

$$A/\tilde{a} \approx s F_g, \tag{9}$$

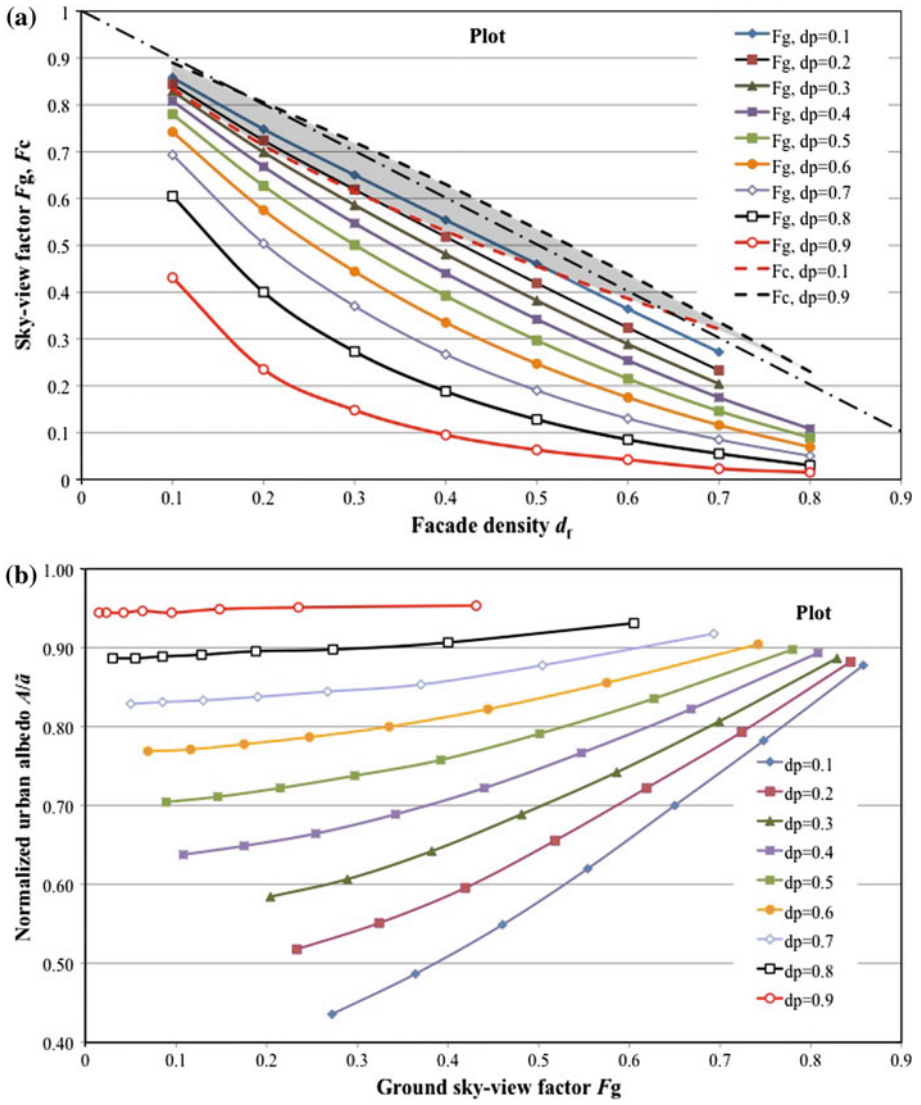

Fig. 4 Mean sky-view factors of the ground surfaces F_g (*solid lines*), and of all canopy surfaces F_c (*dash lines*), as a function of facade density d_f (**a**) (the *grey* surface is the envelope of F_c *curves* and the *thin dash-dot line* represents $F_c = 1 - d_f$), and normalized urban albedo as a function of the ground mean sky-view factor (**b**)

with $s = 0.82(1 - d_p)$. For the high facade densities, where the ground sky-view factor reaches low values (Fig. 4a) the albedo decreases less rapidly with F_g.

It is also interesting to analyse the contributions of the three surface classes to the albedo as a function of densities, by summing the contributions of the facets of each class to the upward solar radiation. The results of Fig. 5 show that the urban albedo is largely constituted by the roofs as soon as the built density exceeds 0.3–0.4. Inversely the ground contribution decreases as the plan density increases, about linearly when the facade density is low but

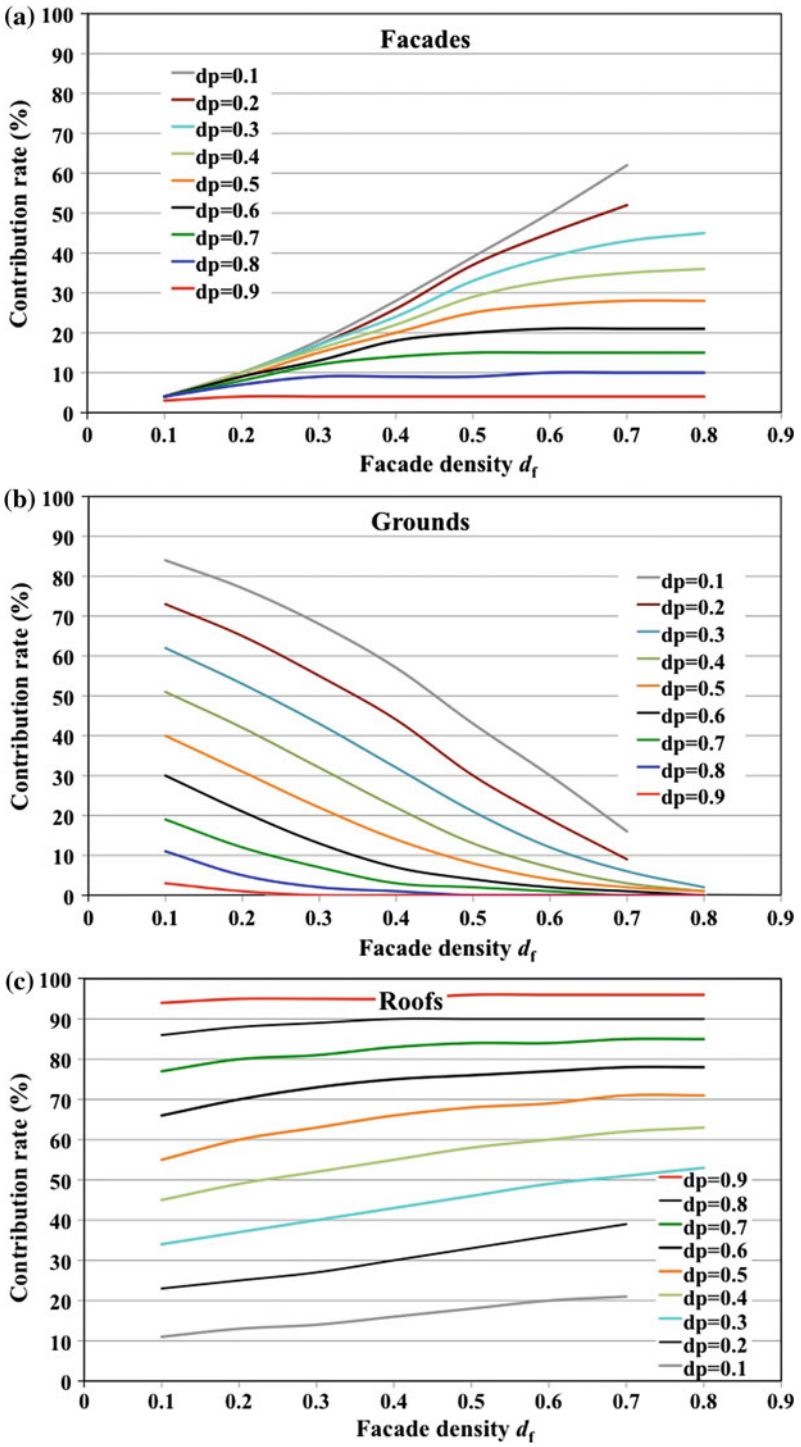

Fig. 5 Relative contributions of the three surface classes to the total solar radiation reflected towards the sky, as a function of facade density for $d_p = 0.1$–0.9, and as a function of plan density for $d_f = 0.2, 0.5, 0.7$

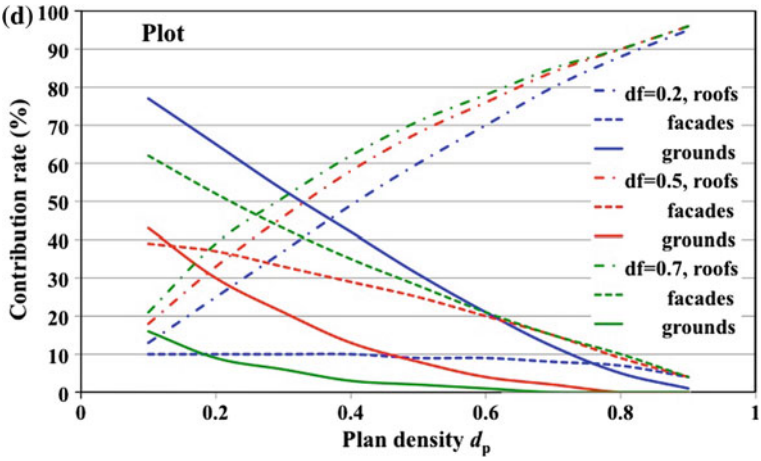

Fig. 5 continued

much more rapidly when d_f is higher. The ground contribution is dominant for the lower plan densities as long as d_f remains low or moderate; for the highest plan densities it is weak. The facades participate weakly to moderately in the urban albedo constitution and their contribution becomes noticeable only when both the built density is low and the facade density is large, reaching an asymptotical value for increasing d_f. We must note here that the uniformity of building heights in the simple Plot configuration, with horizontal roofs, may increase the contribution of roofs compared to real cities, where the roofs of some lower buildings are in the shadow of higher buildings, especially when the plan density is high. We return to this issue below.

3.4 An Empirical Model

The general shape of the curves of Fig. 3, especially their behaviour towards the outer limits, suggests an empirical representation by negative exponentials converging towards $\tilde{a}$ for $d_f = 0$,

$$A = A_\infty + (\tilde{a} - A_\infty) \exp(-C d_f), \tag{10}$$

where A_∞ is the value of the asymptote and both A_∞ and C are functions of d_p. The following empirical functions

$$A_\infty = \tilde{a} d_p^{0.52}, \tag{11a}$$

$$C = 2 - d_p + 10 d_p^2, \tag{11b}$$

have been obtained by fitting these relations to the data of Fig. 3, with a maximum difference of 0.016 between the values of this empirical model and the albedos obtained with SOLENE, a mean bias of 0.0013 and a root-mean-square (r.m.s.) error <0.005. Since A_∞ is proportional to $\tilde{a}$ the empirical model may be written in the following normalized form:

$$A/\tilde{a} = d_p^{0.52} + \left(1 - d_p^{0.52}\right) \exp[-C d_f], \tag{12}$$

with C given by Eq. 11b.

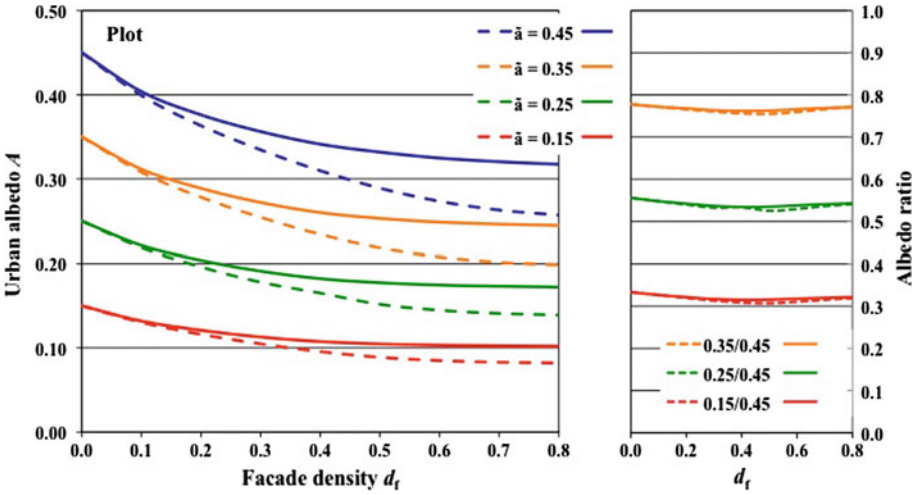

Fig. 6 Albedo variations for four different reflectivities (*left*) and their ratios (*right*) as a function of facade density, for the plan densities $d_p = 0.3$ (*solid lines*) and $d_p = 0.5$ (*dash lines*)

Before proceeding any further we must check if the proportionality between $\tilde{a}$ and A is a reality or an artefact of our representation for $\tilde{a} = 0.45$. Two series of Plot simulations, for $d_p = 0.3$ and 0.5, were repeated for three other values of $\tilde{a}$, 0.35, 0.25 and 0.15. The results appear in Fig. 6 and they show that the albedo variations are homothetic with a ratio $[A(d_f)]_{\tilde{a}}/[A(d_f)]_{0.45}$ practically independent of d_f and equal to $\tilde{a}/0.45$. This justifies the albedo normalization of Eq. 10.

The comparison of Fig. 7 shows that the empirical model represents rather well most of the results obtained with SOLENE but moderately overestimates the albedo for the highest d_f values of the lowest d_p, which correspond to high rise isolated towers. The scale on the right-hand side of Fig. 7 allows us to explain the density influence process also in terms of solar radiation absorption, (i) for all plan densities the absorptivity increment is low when the facade density is low, (ii) for the highest plan densities the increment of solar absorption remains low whatever the value of the facade density and the absorptivity increment rapidly saturates, (iii) for the lower plan densities the absorptivity increment increases continuously with increasing facade density at a rate that increases with decreasing plan density.

3.5 A Revisit of the Results of Kondo et al. (2001), the Influence of Building Height

With their photon tracking method Kondo et al. (2001) computed the albedo of the Plot configuration as a function of building plan density for a fixed building height (cases 1.1–1.6) and as a function of building height for a fixed plan density (cases 2.1–2.6). Cases 1.1 to 1.6 were computed with square buildings with constant height of 25 m and a side length varying from 15 to 40 m on a square mesh of 50 m (four buildings per ha) such that the plan density ranges from 0.09 to 0.64. Their results, presented as albedo daily variations, are somewhat puzzling since these curves criss-cross each other and do not show a clear dependence upon the density. Consequently Kondo et al. did not draw any definitive conclusion on the density influence.

Actually their results show a U-shape variation as a function of d_p as shown in Fig. 8. In this figure the first two solid lines represent the data that were obtained for the summer

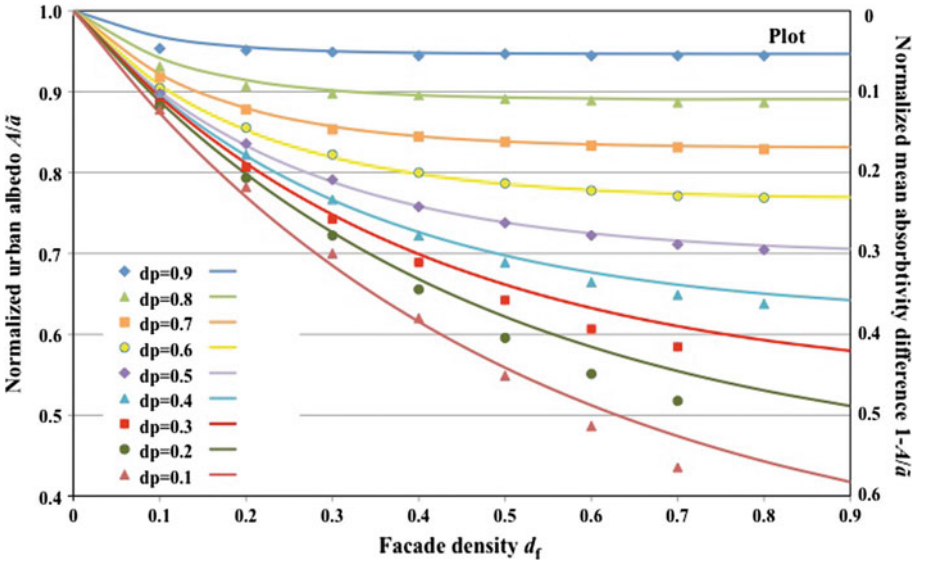

Fig. 7 Urban albedo normalized by the mean reflectivity as a function of plan and facade densities for the Plot configuration: *symbols*, values obtained with SOLENE; *lines*, empirical model

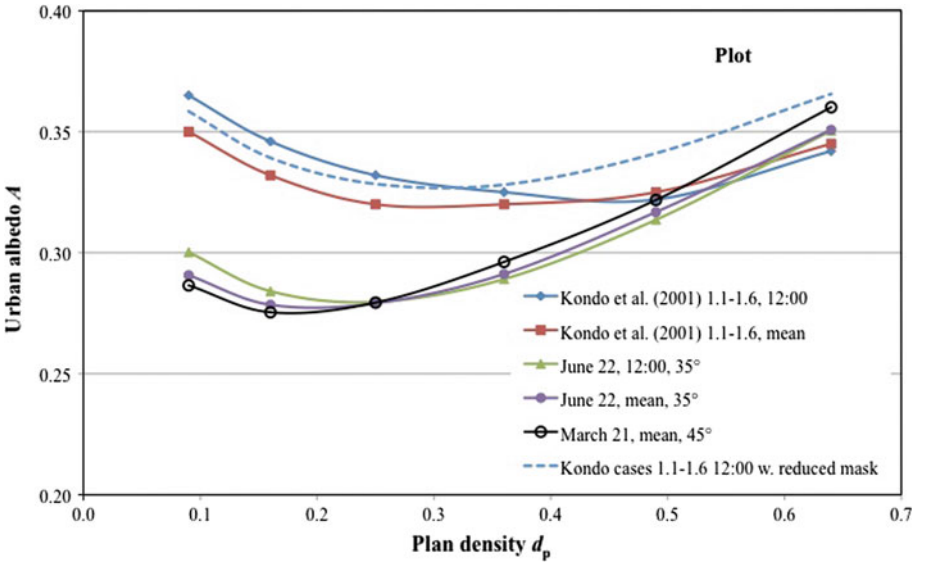

Fig. 8 Urban albedo values obtained by Kondo et al. (2001) for the Plot configuration cases 1.1–1.6, compared to SOLENE results for the same configuration

solstice at the latitude of 35°, respectively at 1200 local time and averaged over the daytime hours (see their Fig. 9). Note that these two curves do not differ much, which is also true for our results of Sect. 3.3. This figure also includes the data obtained with SOLENE in the same conditions for comparison. While they match quite well results of Kondo et al. for the higher densities, they are lower for the lower plan densities. The differences may be

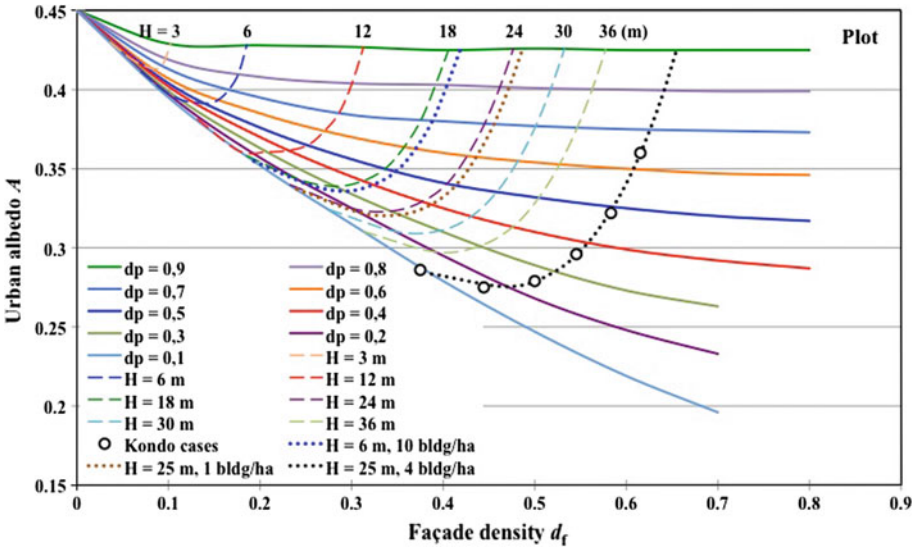

Fig. 9 Same as Fig. 3a with constant building height *curves* for one building per ha (*dash lines*), for different numbers of buildings per ha (*dot lines*), and the configurations 1.1–1.6 of Kondo et al. (2001) (*circles*)

explained by one or several of the following causes: (i) the simplifications that Kondo et al. applied to the photon tracking method for calculating the solar fluxes, (ii) a difference in solar energy repartition between direct and diffuse fluxes, (iii) a difference in reflection properties of surfaces since Kondo et al. consider both mirror (specular) and diffuse reflections while only diffuse reflections are computed by the SOLENE model, (iv) a possible underestimation of the solar masking domain by Kondo et al. To check this last assumption we repeated the simulations with SOLENE in the same conditions as Kondo et al. (35°N, June 22, 1200) but with a reduced mask domain, down to a mask domain identical to the radiosity domain: the dash line shows that this is likely the main reason for the differences between the results of Kondo et al. and ours. The differences are not large and our results show a somewhat similar U-shape, but with a minimum for lower plan densities around 0.2 instead of 0.3–0.5. Finally, the last data in Fig. 8 (black line with circles) show that the results are hardly different for the March equinox. These last data are those that are reported also as black circles in Fig. 3, showing that the U-shape albedo variation with d_p at constant height also appears when displayed as a function of facade density.

To understand this curious, non-monotonous behaviour let us return to the data of Fig. 3 to observe the variation of the albedo as a function of building height. Since for the square Plot configuration the densities and building sizes are related by Eqs. 4 and 5 with $L_x = L_y$, and here $A_T = 1$ ha, we reorder our data as a function of building height and interpolate them to obtain the constant height curves of Fig. 9 (dash lines), with a 3-m step corresponding to the average building level height in Europe. The first observation is that for all plan densities the albedo decreases with increasing building height H (as also observed by Kondo et al. 2001 for $d_p = 0.25$), but at a rate decreasing with the increasing plan density. The second observation is that the curves representing the albedo variations for a constant H all show the U-shape observed in the results of Kondo et al. and our comparisons of Fig. 8. The third observation is that their minimum is displaced towards the low densities when H increases, from $d_p = 0.6$ for $H = 3$ m to $d_p = 0.2$ for $H = 50$ m. These observations demonstrate

that the monotonous variations of the albedo as a function of plan and facade densities are masked when d_f is replaced by H.

Why is the albedo variation with d_p monotonous for constant d_f and not for constant H ? When H increases d_f also increases, which is associated with a decrease in albedo. Inversely, the increasing plan density d_p produces an increase in urban albedo. But the variations are not linear and the influence of d_f (decreasing albedo) is stronger than that of d_p (increasing albedo) for the lower densities. These curves (Fig. 8) highlight two plan density domains: for the low densities the albedo decreases with increasing d_p because of the increasing multiple reflections, while in the high density domain the albedo increases because a larger fraction of solar radiation is directly reflected by the roofs and does not penetrate into the street cavities. The threshold d_p decreases with the increasing H because the higher buildings hinder radiation penetration.

Yet, the plan density and the building height do not suffice to fully define the influence of geometry on the urban albedo: a third variable is required, defining the distribution of buildings and streets in the area. For instance, a given plan density may be obtained with one large building per unit area or with ten buildings ten times smaller in size that yield a much larger facade density if all buildings have the same height (see Eqs. 5 and 6). Therefore, the solid and dash lines of Fig. 9 may be used as an abacus only in the case of 1 building per ha, while the iso-height curves must be re-calculated when the number of buildings per unit area is different, as shown by the dotted lines of Fig. 9. Finally, the iso-height curve for $H = 25$ m with 4 buildings per ha does explain (and extend) the 'curious' distribution of the Kondo case results already shown in Fig. 3.

4 The Urban Albedo for the Canyon Geometry

4.1 The Canyon Configuration

The canyon, or street-canyon, geometry (hereunder 'Canyon') is the second generic form of the urban canopy, constituted of an array of parallel streets of infinite length. Here the unit geometry is a square of side 100 m, with a varying building width according to the urban density, which is repeated on a regular square grid. Since there is no inter-reflections between adjacent streets the simulation geometry includes one complete building row, the two adjacent streets and also the building facades constituting the outer edges of these streets (Fig. 1e). The radiosity domain is 3 units in length and the mask 9 units in length, both of them are 2 units in width. The Canyon configuration is explored for plan densities ranging from 0.1 to 0.9 and facade densities from 0.1 to 0.7, which corresponds to a building height of about 120 m. For two plan densities and two facade densities (0.2 and 0.5) the simulations have been repeated for two orientations (north–south and east–west) and three seasons (December and June solstices and March equinox); the data for the other cases are limited to March 21. All simulations include all daytime hours.

4.2 The Influence of Time, Date and Orientation

Section 3.2 showed that the solar position has a marginal influence on urban albedo in the Plot configuration. The analysis has been repeated for the Canyon configuration: the curves are not shown to save space (but they may be obtained from the authors) since most of the conclusions of Sect. 3.2 may be repeated here, especially as concerns the shape of the

curves. We note in addition that the east–west oriented streets show lower time variations than the north–south streets. We also note that the noon trough appearing for the higher facade densities increases with decreasing plan density; in other words, this trough appears in the north–south streets with the higher buildings and increases with the street width. Although the albedo diurnal amplitude remains on the order of a few % for most cases, it reaches 0.07 in the extreme case ($d_p = 0.2$, $d_f = 0.7$), which corresponds to a variation of $\pm 12.5\,\%$ around the mean. This is obviously larger than for the Plot configuration where the maximum diurnal amplitude reaches 0.04 only and remains lower than 0.02 in most cases (Fig. 2b).

The season and street orientation influences on Canyon albedo are analysed through the mean albedos averaged over all daytime hours, like those of the Plot configuration. The results (not shown for lack of space) may be summarized as follows. The seasonal variations are practically null for the north–south streets (<0.01), and limited to $\pm 2\,\%$ for $d_p = 0.2$ and $\pm 3\,\%$ for $d_p = 0.5$ for the east–west streets; this is slightly more than for the Plot geometry where it is always $< \pm 1.5\,\%$. The orientation influence is also surprisingly low, $< \pm 2\,\%$ for $d_f = 0.2$ and $\pm 3\,\%$ for $d_f = 0.5$, for all seasons. It, therefore, seems that solar angle and layout orientation have very limited influences on the mean urban albedo for the Canyon as well as for the Plot, and probably for any urban morphology, in spite of the noted differences for the largest diurnal variations.

4.3 The Influence of Densities

The facade density is varied from 0.1 to 0.7, beyond which the building height exceeds 120 m and the building height is computed with Eqs. 4–6. In this particular case of infinite street, since $W + W_b$ is constant, Eq. 6 shows that d_f is constant when H is constant, independently of d_p: here iso-height curves are parallel to the ordinate axis. In Fig. 10 they are drawn for the 1-ha square unit, i.e. $W_b + W = 100\,\mathrm{m}$; here also the iso-height lines would be different for another unit area. The general shape of the albedo curves is similar to those of the Plot configuration. For the higher plan densities albedos are very close to those obtained for the Plot configuration while they are higher for the lower densities $d_p \leq 0.5$, such that the empirical model underestimates the values obtained with SOLENE for these low densities when $d_f \geq 0.4$. Actually, the empirical model appears to provide very good albedo estimates for the higher plan densities, for both configurations, and values about midway between Plot and Canyon albedos for the lower plan densities with high facade densities. The convergence of the Plot and Canyon albedos for the higher densities may be explained by the fact that these geometries tend towards rather similar shapes when d_p increases: a high density Plot geometry looks like a grid of perpendicular narrow canyons with smaller and smaller crossroads. In contrast, the systematic difference increases with decreasing density due to the increasing influence of crossroads and cross-streets in the Plot configuration while the infinite Canyon configuration ignores crossroads, as previously noted by Krayenhoff and Voogt (2007). In Fig. 10 the curve for $d_p = 0.01$ correspond to a building reduced to one wall 1-m thick: this indicates the limit of the configuration when the building vanishes but the facade remains.

Can we say that for the high densities the morphological influence on urban albedo is not determinant? In a more general way and inversely, can we conclude that the morphology plays a significant role on urban albedo only when the plan density is low ($< 40\,\%$) and facade density is high ($> 35\,\%$)? It would be of interest to know how many different types of urban form can be built within these limits.

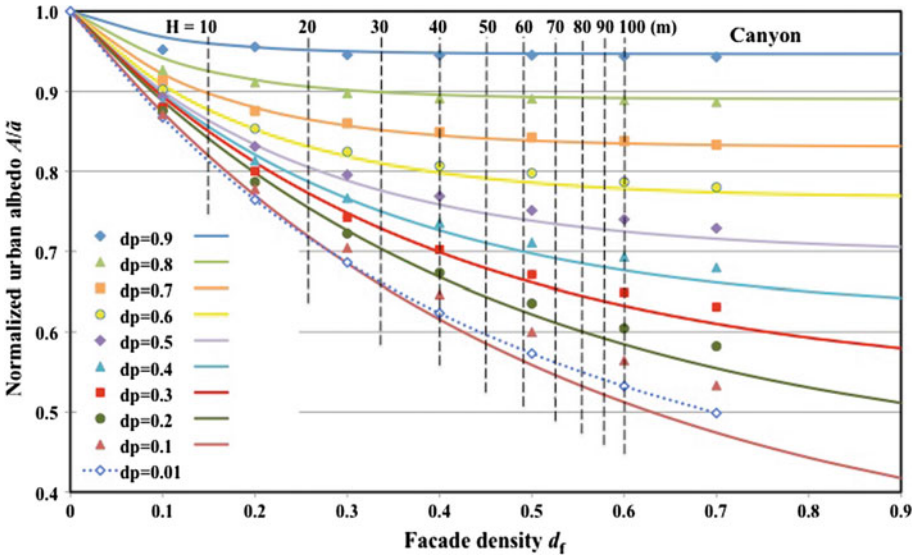

Fig. 10 Urban albedo normalized by the mean reflectivity as a function of plan and facade densities for the Canyon configuration: *symbols*, values obtained with SOLENE; *lines*, empirical model; *dash lines*, constant building height for 1 canyon per ha ($W + W_b = 100\,\text{m}$)

5 The Urban Albedo of Other Geometries

5.1 The Rectangular Plot Geometry

The Plot set-up orientation influence appears surprisingly limited, especially compared to that of the Canyon. To check if this is an artefact due to the symmetrical shape of the square plots, we introduce an intrinsic dissymmetry or a predominant orientation with the rectangular plots (Fig. 1c). Here the urban structure is built on a grid with a square module 100 m on the side, as previously, but with streets two times larger in the rectangle building length direction than in the perpendicular direction as shown in Fig. 1c. The study is limited to two urban densities (0.2 and 0.5) and two facade densities (0.2 and 0.5), but for four orientations of the grid: 0°, 45°, 90° and 145° with respect to north and three dates. The results are presented in Table 1. The analysis of these results leads to the following conclusions:

- the diurnal amplitude (maximum–minimum) never exceeds 0.029 (±4 % variation around the mean);
- for all geometrical cases the difference between the albedos of the different dates does not exceed 0.012 (±1.7 % around the mean);
- for all geometrical cases the difference between the albedos of the different orientations does not exceed 0.005 (±0.7 % around the mean).

These conclusions attest, therefore, to the rather low influence of urban grid orientation with respect to sun direction on urban albedo for the rectangular Plot configuration with avenues two times larger than cross-streets.

The four pairs of squares in Fig. 11 represent the maximum and minimum mean albedo values obtained for each of the four rectangular Plot configurations. They show that the variations with the time of year and orientation are small. The comparison with the Plot

Table 1 Influence of orientation and season on the albedo of rectangular plots; 'dir' indicates the grid orientation, 'mean' is the albedo daytime average and 'amp' its daytime variation amplitude

d_p	dir (deg)	$d_f = 0.2$						$d_f = 0.5$					
		December		March		June		December		March		June	
		Mean	Amp	Mean	Amp	Mean	Amp	Mean	Amp	Mean	Amp	Mean	Amp
0.2	0	0.347	0.015	0.359	0.006	0.359	0.024	0.275	0.006	0.268	0.004	0.271	0.009
0.2	45	0.352	0.017	0.356	0.025	0.358	0.027	0.271	0.014	0.271	0.011	0.270	0.011
0.2	90	0.351	0.020	0.356	0.022	0.356	0.029	0.273	0.009	0.270	0.010	0.272	0.012
0.2	135	0.352	0.017	0.356	0.024	0.358	0.024	0.271	0.014	0.271	0.009	0.270	0.014
0.5	0	0.372	0.009	0.378	0.003	0.378	0.013	0.338	0.011	0.329	0.008	0.329	0.021
0.5	45	0.375	0.008	0.376	0.013	0.377	0.012	0.336	0.009	0.332	0.017	0.331	0.020
0.5	90	0.375	0.011	0.376	0.015	0.377	0.012	0.336	0.015	0.332	0.014	0.330	0.023
0.5	135	0.375	0.009	0.376	0.015	0.378	0.010	0.336	0.008	0.332	0.015	0.331	0.022

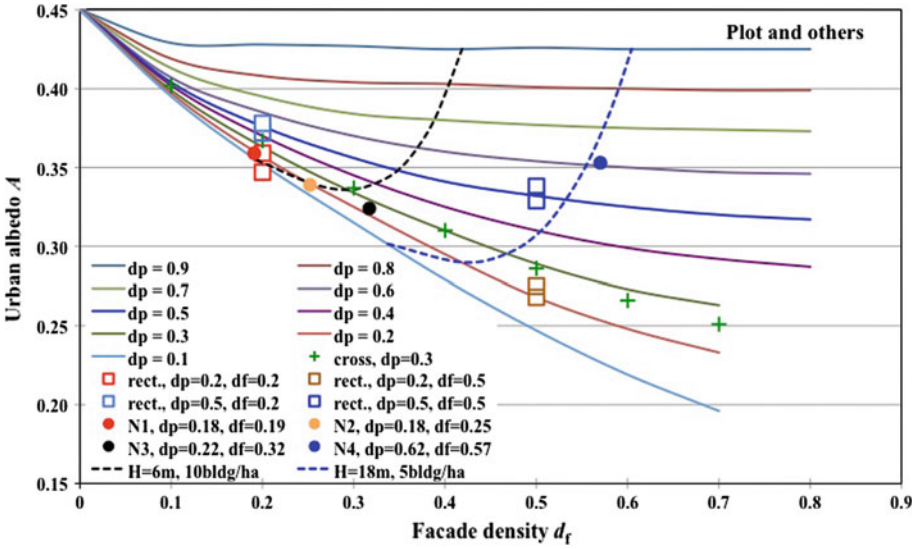

Fig. 11 Same as Fig. 3a with the addition of the mean albedos of the other geometries (see text for details)

albedo curves shows that these results match perfectly the albedos of the square plot geometry for the same densities.

5.2 The Cross Plots

In order to explore further the influence of building shape, another way to modify the facade density consists in modifying the form compactness, using a block whose perimeter is larger than that of the square for the same plan area. This is the case for the simple cross-shaped buildings composed of five equal squares (Fig. 1d). This symmetrical cross has a perimeter $3/\sqrt{5}$ (about 1.34) larger than the square that has the same surface. Therefore, to obtain the same plan and facade densities for the same number of buildings per unit area, the cross

building height must be reduced by a factor of $5^{1/2}/3$, that is to say 0.745, as shown in Fig. 1. This also shows the mask, radiosity and analysis domains, and the computational grid of triangular meshes. These simulations are all performed for $d_p = 0.3$ while d_f varies from 0.2 to 0.7. The mean albedos are reported in Fig. 11 as a series of green crosses, showing that they match nearly perfectly the albedos of square plot geometries for the same densities although slightly lower by 2.5 and 4.5 % for the highest facade densities. The sky-view factors (not shown for lack of space) also match very well the results of Fig. 4. This result confirms the significance of the choice of the facade density as the explanatory variable, rather than building height: the agreement with the (square) Plot albedos would not be very good using the $d_p - H$ set of variables (see Fig. 9) since the cross building heights are 0.745 times lower than those of the square buildings.

5.3 Four Actual Districts of Nantes

Before drawing the conclusions of this study, to assess and confirm them, we consider in this section real urban configurations. The urban agency of Nantes carried out an inventory of urban forms encountered in the Nantes metropolitan area [AURAN, 2008] and selected 68 sites expressing the diversity of urban configurations. A rough statistical analysis shows that 61 % of these sites have a built density <0.20, 29 % have a density between 0.20 and 0.35 and only 9 % have a density >0.35. The maximum density is found in the city centre, as expected. In relation with these densities, two groups of urban morphologies can be identified: the characteristics of the first one are a continuous fabric with relatively high built densities. It represents mainly the classic and traditional urban fabric of European cities with streets, inner courtyards and small public squares, and differs from the Plot and Canyon configurations by the fact that the structure is often not based on a regular grid and includes irregular built blocks. The main characteristic of the second group of morphologies is its discontinuous structure where independent building blocks of various shapes produce an irregular ground coverage and various urban forms. This group includes 'modern' style urbanism with non-aligned buildings and high rise towers, as well as areas with separated individual houses.

Four districts are analysed here, identified below as N1–N4 (Fig. 12). The first three are more or less discontinuous, with relatively low urban densities ($\approx$0.2) and with a rather uniform mean building height of 6 m (two levels or one level with an attic) but with different urban forms. The last one is representative of the continuous urban fabric, with a high urban density, corresponding to a central district constituted of streets continuously bordered with building blocks of 4–6 floors. A uniform building height of 18 m is imposed in the simulations, yielding a mean value of 1.8 for the street aspect ratio H/W. The ground surfaces include not only the streets but also inner courtyards within the blocks. Figure 12 presents their maps, extracted from the cadastre, and their 3D numerical models, built for the simulations. An urban mask with the same type of morphology surrounds the models, simulating an infinite urban fabric. Again, to place in context the morphological influence on urban albedo all the surfaces are assigned the same albedo of 0.45. The morphological parameters are gathered in Table 2, along with the calculation results: sky-view factors and albedos.

The albedo values are reported on the Plot set of curves in Fig. 11. The agreement is again surprisingly good with the albedos of the regular Plot configuration with the same densities $d_p - d_f$. In this figure the dash lines are the iso-height curves corresponding to the building heights and numbers of buildings per ha of the districts N3 and N4. The N4 albedo is not far from the corresponding iso-height curve for $H = 18$ m, five buildings per ha (blue dash line), which is not very surprising since the morphology of the Graslin district is not very

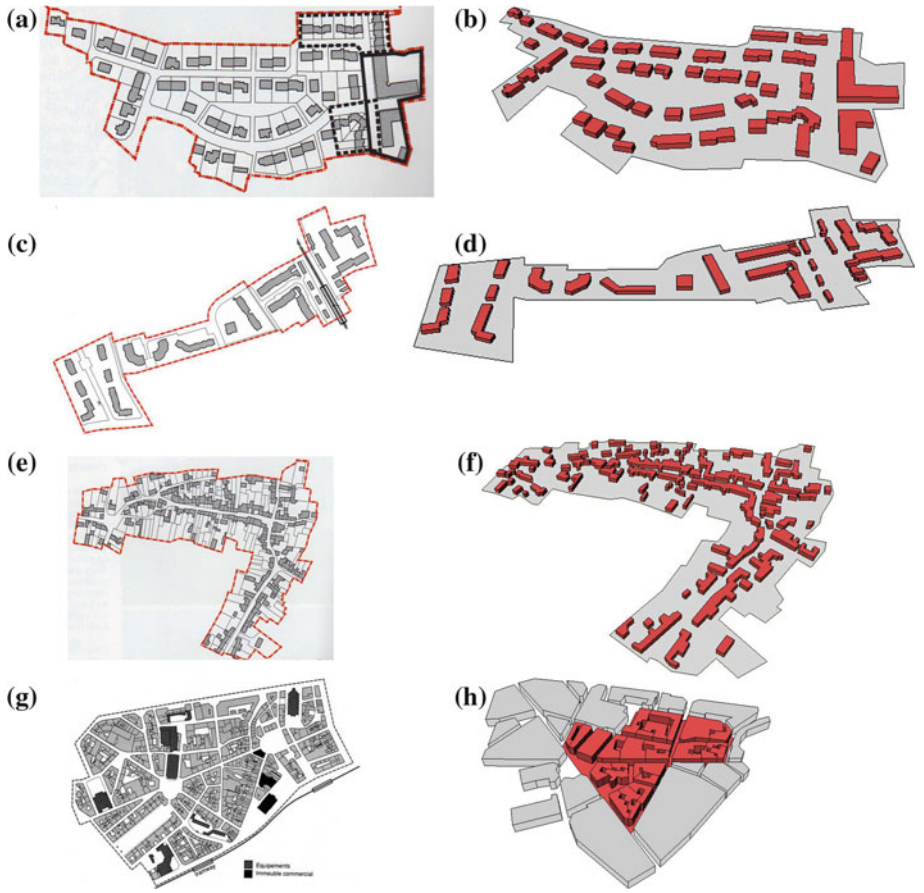

Fig. 12 Maps **a**, **c**, **e**, **g** of the simulated districts of Nantes area and aerial views **b**, **d**, **f**, **h** of their numerical models: districts Douve in Vertou (**a**, **b**), Baugerie in St-Sebastien (**c**, **d**), La Télindière in St Jean de Boiseau (**e**, **f**) and Graslin in Nantes (**g**, **h**), referred in Table 2 as N1–N4, respectively

Table 2 Morphological parameters, sky-view factors and albedos of the four districts of Nantes area

Ref	District name	H (m)	d_p	d_f	n_b (bldg/ha)	F_g	F_c	A
N1	Douve	6	0.185	0.191	3.2	0.74	0.76	0.359
N2	Baugerie	6	0.180	0.252	7.5	0.66	0.66	0.339
N3	La Télindière	6	0.218	0.317	10.0	0.59	0.59	0.324
N4	Graslin	18	0.620	0.570	5.0	0.20	0.44	0.353

different from the Plot configuration (seen to be hardly sensitive to orientation). In contrast, the N3 albedo is relatively far from the corresponding black dash line ($H = 6$ m, 10 buildings per ha), which indicates an albedo of 0.335 for $d_p = 0.218$, instead of 0.324. Likewise the N2 and N1 are very close to this same iso-height curve, therefore relatively far from their corresponding iso-height curves for $H = 6$ m and 7.5 and 3.2 buildings per ha, respectively (not shown for clarity), which would yield higher albedos. This last series of calculations

demonstrates that the albedos of these four real districts are in good agreement with those of the Plot configurations when compared with the $d_p - d_f$ set of variables while they are not with the $d_p - H$ variables. We believe that this conclusion may be generalized to all urban districts.

6 Conclusions

We have analysed the urban albedo mean values obtained in some 270 geometrical configurations, resulting from the averages over all daytime hours for, at least, the March equinox at the latitude of 45° north and several other dates and locations. To focus on the influence of urban morphology on the urban albedo A, all our simulations have been performed with the same reflectivity $\tilde{a}$ for all surfaces. We generally used a reflectivity of 0.45 with respect to the pioneering work of Kondo et al. (2001) but the repetition of some simulations with other values showed an excellent reproduction of the results, allowing us to express our results under the form of the normalized albedo $A/\tilde{a}$.

This study demonstrates that, associated with the commonly used building plan density d_p defined as the ratio of the built to total plan areas, the best explanatory non-dimensional geometrical factor is the facade density d_f defined as the ratio of building facade areas to the sum of all canopy surface areas (roofs, facades and grounds). We show that d_p and d_f play the same roles for all morphologies, either idealized configurations or real districts. We show that, associated with d_p, the building height H is an insufficient descriptor since for a given value of H the albedo varies also with the number of buildings per unit area. Further, we show that d_f is closely related to the mean sky-view factor of the whole canopy surface F_c by the approximate (to within 10 %) simple relationship $F_c \approx 1 - d_f$. Most of our study is based on d_p and d_f but it also includes the influences of solar elevation (time, date and geographical location) and orientation with respect to the urban canopy set-up; we concentrated mainly on the regular (square) Plot configuration but studied also several other idealized configurations (staggered, rectangular and cross plots, infinite street canyons) and several real city districts.

We showed that the solar position has, in general, a marginal influence on the urban albedo, which induces generally small amplitudes of the diurnal variation (r.m.s. $<1.5\,\%$ of the daytime average) and small differences through the seasonal cycle and for different geographical locations. This result has often been hidden in previous studies, either because of experimental artefacts when the sun elevation angle is very low or because numerical simulations were performed with different reflectivity values for facades, roofs and grounds. We explored further the shape of the albedo diurnal variation, showing that it presents a maximum at noon for the lower facade densities d_f, only when the plan density $d_p < 0.8$, while a noon trough appears for the higher densities, more pronounced for the highest facade densities. Also the diurnal variation is less dependent on d_f for the highest plan densities.

This study provides the urban albedo dependency on the plan and facade densities that we expressed with an approximate non-dimensional empirical relationship (Eq. 10). The results are independent of the Plot set-up (regular or staggered) and orientation. The albedo variations as a function of d_f and d_p can be explained in the variations of the respective contributions of the three surface classes (roofs, facades, grounds) to the solar flux reflected towards the sky. These varying contributions also explain why the marginal influence of solar position has been masked in studies where the reflectivities of the surface classes were unequal. The urban albedo is also related to the mean sky-view factor of the ground surface, F_g, showing a tendency towards a linear relationship $A/\tilde{a} \approx s F_g$ for high F_g values (low-to-moderate facade densities) with a slope s proportional to $1 - d_p$ and a lower variation rate for the

higher facade densities for which F_g decreases rapidly. On the basis of these results we have revisited the results of Kondo et al. (2001) and explained their puzzling observation of the non-monotonous albedo variation as a function of d_p for a constant building height.

For the Canyon configuration the albedo variations as a function of d_f and d_p are very similar to those of the Plot configuration, but with higher amplitudes: the difference is null or negligible for the highest plan densities and it progressively increases with decreasing d_p, for the higher facade densities. The negligible differences when the plan density is high may be explained by the relative similitude of the two configurations, since the Canyon geometry mean albedo appears to hardly vary with orientation and also with season. For the lower plan densities the systematic differences are probably due to the absence of crossroads and cross-streets in the Canyon configuration, which shows an absolute directivity. This is also the reason for the relatively large amplitudes of the albedo diurnal variations of the high north–south canyons, which increase with the decreasing built density or increasing street width.

The very low influence of orientation is also assessed from the results obtained with the regular configuration of rectangular plots with avenues twice as wide as cross-streets. The mean albedo values of the rectangular plots agree perfectly with those of the square plots for the same values of the couple of densities d_f and d_p. The cross plots show the same agreement although cross-shaped buildings present a 34 % larger surface of facades than the square buildings of the same height and plan area. Finally, the albedo obtained for four actual districts typical of the morphologies observed in the Nantes urban area also agree quite well with the Plot albedo curves. These last calculations demonstrate that the agreement is probably general for all urban forms.

To return to our original question, do these results imply that the urban form has no influence on the albedo? The answer is negative if the form is defined by the most straightforward parameters such as building height, in which case the albedo depends on other morphological parameters such as the number of buildings per unit area and the relationships are not simple. But it seems that the plan and facade densities fully define nicely the morphology influence on the albedo for any geometry, with the exception of the pure idealized Canyon configuration that shows higher albedos for the lower plan densities and the higher heights or facade densities.

This conclusion may be limited to configurations with constant building heights. Kondo et al. (2001) showed for one Plot configuration that the albedo decreases slightly when the building height is not uniform, the roofs of some lower buildings being in the shadow of higher buildings. Building height inhomogeneity seems a secondary factor of influence, but it may deserve further investigation.

It is our experience of the architectural design process that the form is designed before the choice of the materials and colours. We believe that, although approximate, our empirical model, which is composed of simple mathematical expressions, will be useful to predict as early as possible in this design process the influence of the architectural form on the energy budget and the energy absorbed by the buildings.

Let us finally note that the urban heat island is commonly associated with higher densities of taller buildings because these would increase solar radiation trapping. Our study shows, on the contrary, that when the built density is large the influence of roofs on the albedo becomes largely dominant, nearly independently of facade density or building height, and that the increment of absorptivity (due to the canopy geometry) remains small. The increasing heat island with increasing density is thus probably much more influenced by the heat released by anthropogenic energy consumption, which does increase with the built density, and by the increasing heat storage capacity of high building walls.

Acknowledgments Part of this work has been done when the second author was working with the Laboratory of Fluid Mechanics of the Ecole Centrale de Nantes (UMR CNRS 6598).

References

Aida M (1982) Urban albedo as a function of the urban structure—a model experiment. Boundary-Layer Meteorol 23:405–413

Aida M, Gotoh K (1982) Urban albedo as a function of the urban structure—a two-dimensional numerical simulation. Boundary-Layer Meteorol 23:415–424

Arnfield AJ (1988) Validation of an estimation model for urban surface albedo. Phys Geogr 9:361–372

Arnfield AJ (2000) A simple model of urban canyon energy budget and its validation. Phys Geogr 21:305–326

AURAN (2005) Quartiers de villes, Quartiers de vie, Habitat et Formes urbaines (in French). Urbanism agency of the Nantes urban area, 165 pp. www.auran.org/

Christen A (2005) Atmospheric turbulence and surface energy exchange in urban environments: results from the Basel Urban Boundary Layer Experiment (BUBBLE). Doctoral Thesis, Basel University, 140 pp

Grimmond CSB, Salmond JA, Oke TR, Offerle B, Lemonsu A (2004) Flux and turbulence measurements at a densely built-up site in Marseille : heat, mass (water and carbon dioxide), and momentum. J Geophys Res 109:D24101. doi:10.1029/2004JD004936

Groleau D, Fragnaud F, Rosant J-M (2003) Simulation of the radiative behaviour of an urban quarter of Marseille with the SOLENE model. In: Klysik K, Oke TR, Fortuniak K, Grimmond CSB, Wibig J (eds) Proceedings of fifth international conference on urban climate, Lódz, Poland

Hénon A, Mestayer PG, Groleau D, Voogt JA (2011) High resolution thermo-radiative modeling of an urban fragment in Marseilles city center during the UBL-ESCOMPTE campaign. Build Environ 46:1747–1764

Hénon A, Mestayer PG, Lagouarde JP, Voogt JA (2012) An urban neighborhood temperature and energy study from the CAPITOUL experiment with the S olene model. Part 1: analysis of flux contributions. Theor Appl Clim. doi:10.1007/s00704-012-0616-z

Idczak M, Groleau D, Mestayer P, Rosant JM, Sini JF (2010) An application of the thermo-radiative model SOLENE for the evaluation of street canyon energy. Build Environ 45:1262–1275

Kanda M, Kawai T, Nakagawa K (2005) Simple theoretical radiation scheme for regular building arrays. Boundary-Layer Meteorol 114:71–90

Kondo A, Ueno M, Kaga A (2001) The influence of urban canopy configuration on urban albedo. Boundary-Layer Meteorol 100:225–242

Krayenhoff ES, Voogt JA (2007) A microscale three-dimensional urban energy balance model for studying surface temperatures. Boundary-Layer Meteorol 123:433–461

Masson V (2000) A physically-based scheme for the urban energy balance in atmospheric models. Boundary-Layer Meteorol 94:357–397

Masson V (2006) Urban surface modelling and the meso-scale impact of cities. Theor Appl Climatol 84:35–45

Masson V, Gomes L, Pigeon G, Liousse C, Pont V, Lagouarde JP, Voogt J, Salmond J, Oke TR, Hidalgo J, Legain D, Garrouste O, Lac C, Connan O, Briottet X, Lachérade S, Tulet P (2008) The Canopy and Aerosol Particles Interactions in TOulouse Urban Layer (CAPITOUL) experiment. Meteorol Atmos Phys 102:135–157

Miguet F, Groleau D (2002) A daylight simulation tool for urban and architectural spaces—application to transmitted direct and diffuse light through glazing. Build Environ 37:833–843

Oke TR (1987) Boundary layer climates, 2nd edn. Methuen and Co. Ltd., London, 435 pp

Oke TR (1988) Street design and urban canopy layer climate. Energy Buildings 11:103–113

Pawlak W, Fortuniak K (2002) Estimation of the effective albedo of the urban canyon—comparison of the two different algorithms. In: International conference “Man and climate in the 20th century”, Wroclaw, 13–15 June 2002

Perez R, Seals R, Michalsky J. (1993) An all-weather model for sky luminance distribution. Solar Energy 50:235–245

Pigeon G, Moscicki MA, Voogt JA, Masson V (2008) Simulation of fall and winter surface energy balance over a dense urban area using the TEB scheme. Meteorol Atmos Phys 102:159–171

Sievers U, Zdunkowski W (1985) A numerical simulation scheme for the albedo of city street canyons. Boundary-Layer Meteorol 33:245–257

Vinet J (2000) Contribution à la modélisation thermo-aéraulique du microclimat urbain. Doctoral thesis (in French), Ecole Centrale de Nantes and Nantes University, Nantes, France, Caractérisation de l’impact de l’eau et de la végétation sur les conditions de confort en espaces extérieurs, 245 pp